Physics of Plasmas ARTICLE scitation.org/journal/php

Evolution of a shock wave generated by underwater electrical explosion of a single wire

Cite as: Phys. Plasmas **26**, 042302 (2019); doi: 10.1063/1.5092321
Submitted: 10 February 2019 · Accepted: 25 March 2019 ·
Published Online: 16 April 2019

A. Rososhek, S. Efimov, V. Gurovich, A. Virozub, S. V. Tewari, and Ya. E. Krasik

AFFILIATIONS

Physics Department, Technion, Haifa 3200003, Israel

ABSTRACT

The results of an experimental, analytical, and numerical study of the cylindrical shock wave generated by the underwater electrical explosion of copper and aluminum wires are reported. Experiments were conducted using a microsecond timescale generator delivering ~180 kA pulses with a 1.2 μs rise time. Shadow streak images were used to study the radial expansion of the exploding wire and the generated shock wave. It was found that the shock wave expansion velocity decreases to the velocity of sound in two stages: a fast stage and then a gradual stage. The fast stage occurs during ~1.5 μs after the maximum of the resistive voltage is reached, and then, a gradual decrease occurs during several tens of microseconds. It was shown that the duration of the fast stage corresponds to the period of time when the main energy deposition into the wire occurs. Hydrodynamic simulations show that the fast decrease in the shock velocity is related to the evolution of the exploded wire's subsonic expansion, which leads to time/spatial compression of the adjacent water layer. For the gradual decrease stage of the shock wave velocity, we developed a simplified model, which considers uniform water density between the wire boundary and the shock wave front. The results of this model agree satisfactorily with the experimentally obtained shock wave trajectory and radial expansion of the wire.

I. INTRODUCTION

High energy density physics and warm dense matter[1] attract considerable attention because of their relevance to both theoretical and experimental studies of material properties at the extreme conditions found in astrophysics,[2] planetary science,[3] and inertial confinement fusion.[4] Laboratory studies are important for validation of equations of state (EOS) and developing conductivity models. Shock wave studies have been a part of this subject for more than 70 years, enabling researchers to achieve warm dense matter in laboratory conditions.[5,6] Different methods for generating shock waves exist, such as gas guns,[7] laser radiation techniques,[8,9] and electrical explosions of conductors or discharges in different insulator media.[10] In one of the first theoretical studies by Taylor (1950)[11] related to a blast wave, an instantaneous release of finite energy confined in an infinitely small space was considered and the so-called square root model for the shock wave trajectory was obtained for the first time. An analytical solution for blast-wave propagation was later considered independently by Sedov[12] and von Neumann.[13] Thereafter, the shock wave implosion problem was solved by Guderley,[14] Landau,[15] and Stanyukovich.[16] All these theoretical approaches considered a self-similar motion of the shock wave without taking into account the dynamics of the piston that initially generates this shock.

In the 1950s, Sakurai[17,18] and Lin[19] adopted Taylor's approach for describing a divergent cylindrical shock wave. To test their treatment, Bennett[20] used exploding wires and investigated the dynamics of the generated shock wave in air using a reflecting mirror with a streak camera to obtain the shock wave trajectory. Another group led by Jones utilized the self-similar approach to describe a shock wave generated by lightning discharge[21] and inverse pinch.[22] A detailed study of an expanding spark channel in different liquids and observations of the shock waves were performed by Skvortsov *et al.*[23] and Krivitskiy *et al.*[24] In this research, the electrical discharge in water was described using the so-called similarity parameters,[25–27] providing additional tools for characterizing the discharge process.

In the late 1990s, De Silva[28] suggested using an electrical wire explosion in water to study the electrical conductivity of dense plasmas. The main advantages of using water as a medium for wire explosion are the high voltage breakdown threshold, which prevents plasma flashover along the wire surface, and the relatively slow radial expansion of the wire due to the low compressibility of water. This allows one to maintain high energy density deposition, and the transparency of water allows streak cameras to be used to take images of the exploded wires and the generated shock waves.

During the last two decades, strong shock wave generation by an underwater electrical wire explosion in the 10^{-7}–10^{-6} s timescale was studied worldwide. The main research goals were to verify the EOS and conductivity models for the exploding wire materials under

extreme conditions. Additionally, different approaches involving shock waves were investigated as part of the research on inertial confinement fusion or destruction of solid materials.[29] As a result, primary attention was given to the implosion problem and shock wave uniformity in different geometries, cylindrical,[30,31] spherical,[32,33] and ring.[34] Less attention has been paid to divergent shock wave dynamics, which was described using self-similar solutions that assume instantaneous energy release, neglecting the piston motion.

The main objective of the present study was to develop a simplified model that describes divergent shock propagation without assuming self-similarity and instantaneous energy release and to compare this simplified model with experimental results. We show that the shock wave and exploding wire radial expansions observed in shadow streak images agree satisfactorily with the model. In addition, we performed one-dimensional (1D) hydrodynamic (HD) simulations[35] coupled with the EOS for water and the wire material. The results of these simulations are in good agreement with the model and show the initial stage of the shock wave generation by the expanding wire with subsonic velocity while the main energy deposition into the wire occurs.

This paper is divided into five parts. The simplified model is described in Sec. I. In Sec. II, we describe the experimental setup and in Sec. III our results. In Sec. IV, we present the results of the model and the HD simulations and compare them to the experimental results. A summary is presented in Sec. V.

II. SIMPLIFIED MODEL OF THE DIVERGENT CYLINDRICAL SHOCK WAVE

Let us consider the underwater electrical explosion of a single wire characterized by the critically damped discharge which allows almost all the energy stored in the pulse generator be deposited into the wire during a time smaller than a quarter-period in the case of underdamped discharge. During the explosion, the wire experiences solid-state–liquid–vapor–low-ionized plasma phase transitions, accompanied by a change in the wire volume, and consequently, by the formation of a shock wave in the water. However, solid-state–liquid–vapor transitions lead to the formation of a weak shock. A strong shock wave is generated during the vapor–low-ionized plasma phase transition when the main energy deposition is realized, leading to fast radial expansion of the exploded wire plasma channel (cavity). Typical pressures realized at the cavity–water boundary for the experimental conditions under consideration do not exceed 10^{10} Pa,[36,37] allowing the use a polytropic equation of state[5] for water at that location

$$P(\delta) = \frac{\rho_0 c_0^2}{n}[\delta^n - 1], \tag{1}$$

where $c_0 = 1496.8\,\mathrm{m/s}$[38] is the velocity of sound in undisturbed water at ~296 K, $n = 7.15$ is the polytropic index for water, $\delta(t) \equiv \rho(t)/\rho_0$ is the water compression parameter, and $\rho(t)$ and ρ_0 are the densities of water behind and in front of the shock, respectively.

To define the velocity of the shock wave front $D = dR_{sw}/dt$ where $R_{sw}(t)$ is the radius of the shock wave front relative to the wire axis, one must know the water compression parameter $\delta(t)$ behind its front. Indeed, the value of $\delta(t)$ determines the velocity of the shock as

$$\frac{dR_{sw}}{dt} \equiv D = \sqrt{\frac{c_0^2}{n}\frac{(\delta^n - 1)\delta}{\delta - 1}}. \tag{2}$$

In general, the density of the water inside the layer between the shock front and cavity boundary, ρ, is a function of both time and space. In our simplified model, we assume that the density of the water inside this layer is uniform, implying that ρ is only a function of time. It is understood that this assumption requires justification, and hence, it is addressed in Sec. IV.

Let us define $R_{ch}(t)$ as the radius of the expanding cavity relative to the wire axis. The mass of the compressed water inside the layer between $R_{sw}(t)$ and $R_{ch}(t)$ is

$$M(t) = \pi\left[R_{sw}^2(t) - R_{ch}^2(t)\right]L\rho(t), \tag{3}$$

where L is the length of the cavity. The water mass change rate is dictated by the water penetrating into the compressed layer through the shock wave front. Thus, equating the time derivative of Eq. (3) with that of the mass of water entering the compressed layer through the shock wave front $2\pi L\rho_0 R_{sw}(dR_{sw}/dt)$, one obtains an equation for the time evolution of the water compression inside the layer

$$\frac{d\delta}{dt} = \frac{2\delta\left(R_{ch}\frac{dR_{ch}}{dt} - R_{sw}\frac{dR_{sw}}{dt}\right) + 2R_{sw}\frac{dR_{sw}}{dt}}{R_{sw}^2 - R_{ch}^2}. \tag{4}$$

The solutions of Eqs. (2) and (4) define the value $D(t)$ for the known cavity expansion velocity dR_{ch}/dt. The latter can be determined by equating the electrical power $W(t)$ deposited into the cavity of volume $V(t) = \pi LR_{ch}^2(t)$ with the sum of the cavity internal energy density U and the work produced by the pressure P at the cavity–water boundary. Assuming that low-ionized plasma inside the cavity can be considered an ideal gas, $U = (3/2)P$. This allows us to write

$$2\eta W(t) = 3V(t)\frac{dP}{d\delta}\frac{d\delta}{dt} + 10P(t)\pi LR_{ch}(t)\frac{dR_{ch}}{dt}, \tag{5}$$

where η is the part of the deposited electrical power converted into the heat and work for the water flow generation by the cavity expansion. Next, using Eq. (1), one obtains

$$2\eta W(t) = 3\pi LR_{ch}^2(t)\rho_0 c_0^2\delta^{n-1}\frac{d\delta}{dt} + 10\pi L\frac{\rho_0 c_0^2}{n}(\delta^n - 1)R_{ch}(t)\frac{dR_{ch}}{dt}. \tag{6}$$

The solutions of Eqs. (2), (4), and (6) using measured $W(t)$ and η as input parameters allow us to obtain the evolution of $R_{ch}(t)$, $R_{sw}(t)$, and $\delta(t)$, and, consequently, the shock wave velocity. A comparison of this simplified model with experimental and HD simulation results is presented in Sec. IV.

III. EXPERIMENTAL SETUP

The experiments were conducted using a microsecond timescale high-current generator.[39] The generator consists of four low-inductance high-voltage Maxwell type capacitors, connected in parallel with the total capacitance of 10 μF, charged to 25 kV resulting in an initially stored energy of ~3.12 kJ. Each capacitor is discharged by a multi-electrode spark gas switch triggered by a Maxwell generator 40230 producing a 70 kV, 15 ns long output pulse with a time jitter of ~2 ns. The rise time of the discharge current on a short-circuit load of inductance similar to that of the exploding wire is ~1200 ns. The total inductance and resistance of the discharge circuit are ~65 nH and ~0.01 Ω, respectively. Hereinafter, the terms Cu 600 and Al 800 are

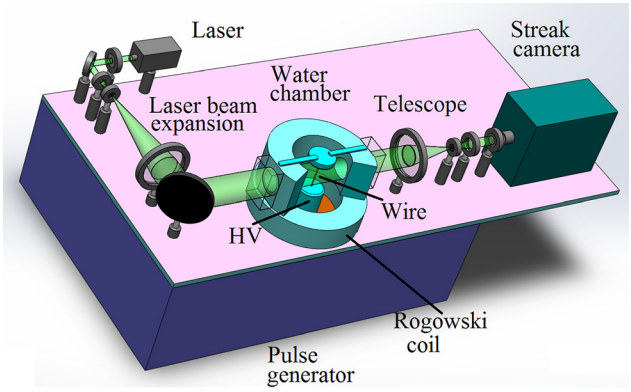

FIG. 1. Experimental setup.

used to refer to copper and aluminum wires having diameters of 600 μm and 800 μm, respectively. The length of the wires was 45 mm. The choice of this parameter allows us to obtain almost critically overdamped discharge characterized by the fastest stored energy transfer to the exploding wire (see Sec. II). The wire was stretched between a grounded and a high-voltage electrode placed inside a stainless-steel chamber (see Fig. 1) filled with de-ionized water.

The discharge current I_d through the wire was measured using a self-integrated Rogowski coil ($\pm$5% error), and the voltage drop φ along the wire was measured by a Tektronix voltage divider ($\pm$1% error) connected to the high-voltage electrode. For the exploding wire backlighting, we used a 155 mW diode-pumped, 532 nm CW laser (MGL-III-532). The shadow images were obtained with a streak camera (Optoscope SC-10) operating with streak durations in the range of 1–20 μs. Time synchronization between the generator and streak camera was performed by a Stanford Digital Delay Generator DG645, which also triggered the fast light emitting diode to produce a marker at the streak image. The error in determining the time in streak images was found to be $\pm$15 ns. At least two shots of the generator were executed for each wire, showing reproducible waveforms of the discharge current and voltage and repeatable shadow images of the exploding wire. We estimate average errors of $\pm$7.5% and $\pm$10% in an analysis of the shock wave and cavity trajectories, arising from non-ideal optical alignment, finite density contrast, and streak nonlinearity.

IV. EXPERIMENTAL RESULTS

Explosions of Cu 600 and Al 800 wires are characterized by almost critically damped discharges with similar amplitudes and waveforms of the discharge current and resistive voltage $\varphi_R = \varphi - L_{load}(dI_d/dt)$, where $L_{load} \approx 12$ nH is the load inductance determined in short-circuit experiments. In Fig. 2, we present waveforms of the discharge current, resistive voltage, power, and energy deposition to the exploding wires. The main parameters of these explosions are shown in Table I. One can see that the discharge currents reach a maximal amplitude of ~180 kA at almost the same time, ~1150 ns, and the main energy deposition into the wire occurs during ~1 μs. The efficiency of the initially stored energy in the generator transfer to the exploding wires in these explosions is ~75%.

Typical shadow streak images for Cu 600 and Al 800 explosions overlapped with the deposited power ($t = 0$ is related to the beginning of the discharge current) are shown in Fig. 3. Spatial and temporal resolutions are identical in these images, namely, ~37 μm/pixel and ~14.4 ns/pixel, respectively. One can see the initial wires prior to the

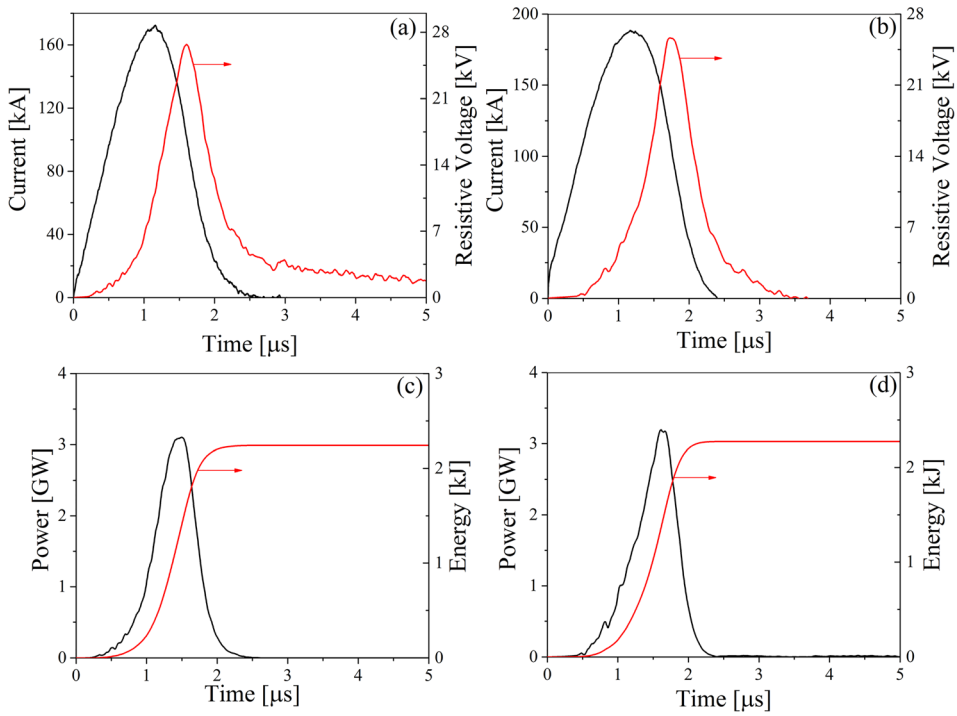

FIG. 2. Waveforms of the discharge current, resistive voltage, power, and energy deposition obtained in explosions of Cu 600 [(a) and (c)] and Al 800 [(b) and (d)].

TABLE I. Main wire explosion parameters.

Material	Current rise-time [ns]	Current amplitude [kA]	Resistive voltage amplitude [kV]	Resistance at the voltage maximum [Ω]	Deposited energy [kJ]	Maximal power [GW]
Copper 600 μm	1150	172 ± 9	27 ± 0.3	0.26 ± 0.01	2.45	3.7
Aluminum 800 μm	1150	188 ± 10	26 ± 0.3	0.22 ± 0.01	2.28	3.2

beginning of the discharge current followed by bright self-emission from the exploded plasma becoming visible, in spite of the narrow band (1 nm) interference 532 nm-filter placed in front of the input slit of the streak camera. The duration of this bright emission is roughly equal to the period during which the main energy density deposition into the wire occurs. One can also see that the fast expansion of the cavity, and consequently the generation of the strong shock wave (at that time we can resolve neither the cavity nor the shock wave), appears at the beginning of the fast rise in the deposited power, i.e., when one obtains the vapor–low-ionized plasma phase transition. Detailed studies of this stage and stages where solid-state–liquid–vapor phase transitions occur were presented in Ref. 40. Finally, at $t \geq 2.5$ μs, when the main power deposition is already terminated and the expanding cavity can be considered low-ionized gas, one obtains a significantly slower expansion of the cavity, accompanied by the fast radial expansion of the shock wave and a rather turbulent compressed water layer between the cavity boundary and shockwave front.

Analysis of the shadow streak images allows one to obtain the shock wave and cavity expansion trajectories from the inflection point (see Fig. 3). From that point, using markers with a constant time step, the shock wave front and cavity boundary were analyzed to the last clearly resolvable point. The results of this analysis, together with the calculated shock wave front and cavity expansion velocities, are shown in Fig. 4. One can see that there are two stages in the evolution of the shock wave velocity. Namely, first a sharp decrease in the velocity is seen during the first ~1.5 μs from the time of the maximum discharge current. This stage transforms to a slow decrease in the shock velocity gradually approaching the speed of sound in undisturbed water. A qualitatively similar evolution is obtained for the cavity expansion velocity. In addition, one can see that the rise in the shock and cavity velocities occurs at approximately the same time.

Here, let us note small differences in the temporal evolution of shock and cavity velocities for the Al 800 and Cu 600 explosions. For Al 800 wire explosions, one obtains a slower decay in shock and cavity velocities than for Cu 600 wire explosion. This can be related to the slightly different explosion parameters (see Table I), as well as to the possible combustion of Al wires delivering additional energy to the expanding cavity and generated water flow. Nevertheless, despite this difference, at $t \approx 16$ μs, the shock waves for both Cu 600 and Al 800 wire explosions approach the same radius, namely, $r \approx 27.6 \pm 1.3$ mm and $r \approx 28.0 \pm 1.3$ mm, respectively. In addition, for example, for Cu 600 wire explosions, the maximal resolvable shock velocity has a value of $\approx 3 \times 10^5$ cm/s obtained at $t \approx 2.450 \pm 0.015$ μs and $r \approx 2.88 \pm 0.58$ mm, which results in a pressure of $\sim 2.3 \times 10^9$ Pa and a water density of ~ 1.35 g/cm^3 behind the shock wave front.

V. DISCUSSION

The experimental results show that strong shock wave generation starts when the wire experiences the vapor–low-ionized plasma phase transition, characterized by a fast increase in the resistance ($\sim 3 \times 10^5$ Ω/s) and the beginning of the main energy deposition into the wire. A drastic (during $\sim 10^{-7}$ s) increase in the temperature of the wire up to $\geq 10^4$ K leads to a rapid increase in its volume. The latter results in a significant compression of water in the vicinity of the expanding wire and the generation of a strong shock. Because of the high velocity of $\sim 3 \times 10^5$ cm/s acquired by the shock during the fast cavity expansion stage when the main energy deposition occurs, the shock departs from the cavity, which at that time decreases its velocity because the energy deposition is terminated. The latter leads to a fast decrease in the shock velocity from $\sim 3 \times 10^5$ cm/s to $\sim 2.1 \times 10^5$ cm/s within ~1.5 μs. This fast decrease in the shock velocity transforms to a slower gradual decrease down to $\sim 1.65 \times 10^5$ cm/s during the next 14 μs. One can

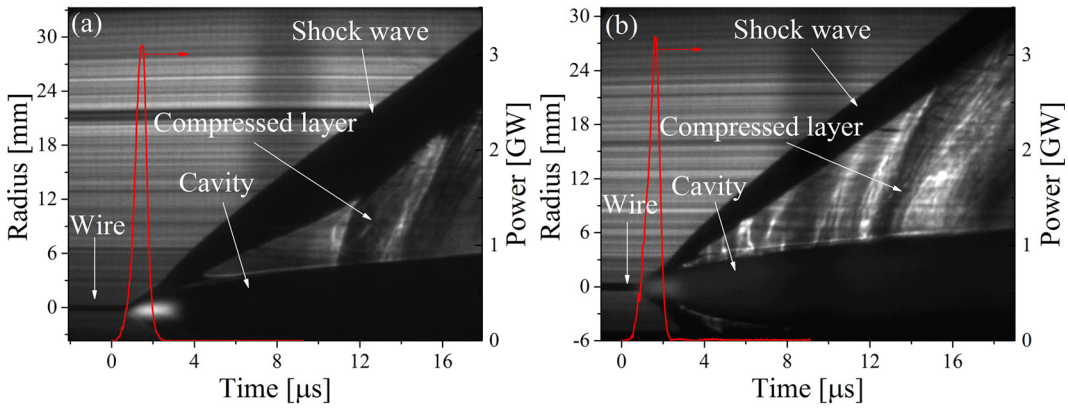

FIG. 3. Shadow streak images for Cu 600 (a) and Al 800 (b) wire explosions overlapped with the deposited power.

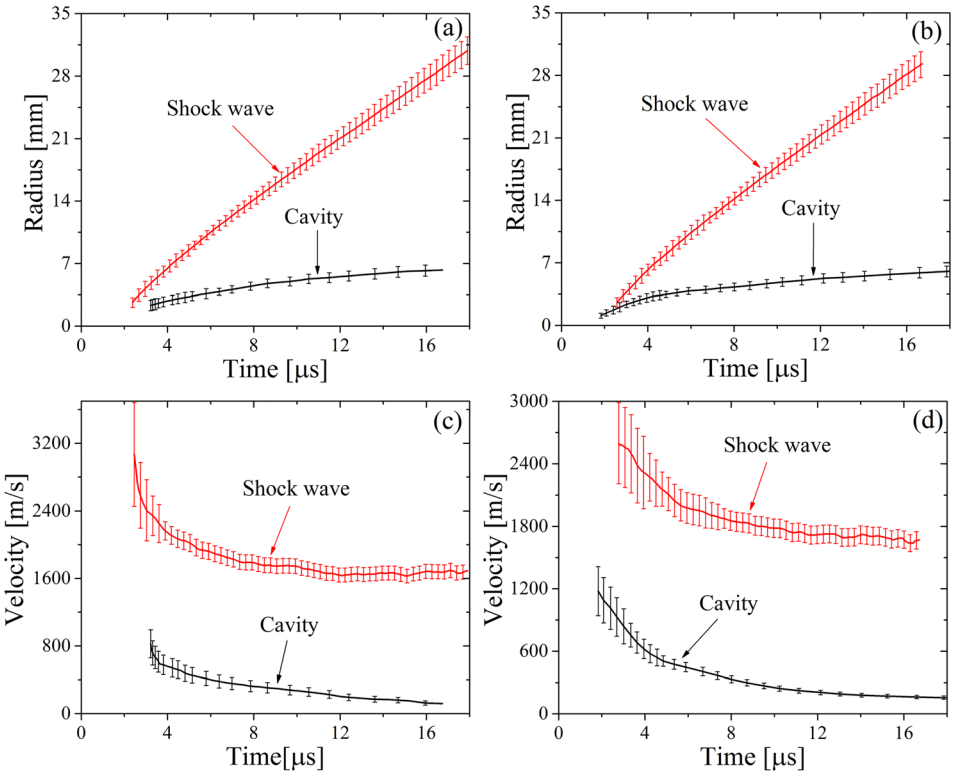

FIG. 4. Shock wave trajectory and velocity; the channel expansion and velocity for Cu 600 [(a) and (c)] and Al 800 [(b) and (d)] wire explosions.

consider that the slow stage of the shock expansion is associated with the cavity's continuing radial expansion. The latter pushes the water layer, supplying the shock with additional energy, because the sound velocity in the compressed water is greater than the shock wave velocity.

Now, let us compare the experimental data with the simplified model described in Sec. II and 1D HD simulations[41,42] coupled with SESAME EOS for water, copper, and aluminum[35] using the measured time-dependent electric power as input. The simulation results are verified by computing the total energy transferred into the water flow, which must be bounded by 24%[43] and by matching the simulated with the experimentally obtained shock wave trajectory.

A comparison of the shock and cavity trajectories and velocities obtained experimentally by 1D HD simulations and by the simplified model is shown in Fig. 5. One can see a rather good agreement between the simplified model and the experimentally measured shock wave and cavity trajectories together with the calculated velocities. Only during $2\ \mu s < t < 4\ \mu s$, which corresponds to the fast decrease in the shock velocity stage, one can see some difference between the model and the experimental results. A similar agreement between the experiment and the model was obtained for the Al 800 wire explosion, except for a more pronounced difference in the cavity expansion at times $t < 4.5\ \mu s$. Further, one can see that the shock velocity (for both the Cu 600 and Al 800 wire explosions) converges asymptotically ($t \gg 20\ \mu s$) to the sound velocity, as predicted by the model.

However, one can see that, at $t < 3\ \mu s$, the results of the 1D HD modeling of shock wave trajectory do not fit the experimental data well. This can be related to the uncertainty in the determination of the shock wave front position and cavity boundary at early times.

The 1D HD simulation shows that the cavity expansion velocity does not reach the speed of sound in undisturbed water during the time of the main energy deposition into the wire. In addition, even accounting for large errors at late times, the extrapolated experimental data of the shock wave trajectory show that the maximal velocity of the cavity expansion does not exceed 1450 m/s. Thus, the generation of the shock wave occurs because of the formation of the compressed water layer in the wire's vicinity by the cavity expansion. At the beginning of this process, this density disturbance propagates outward from the wire at the velocity of sound. However, cavity expansion with increasing velocity [see Figs. 5(c) and 5(d)] leads to further water layer compression, which propagates through the compressed water with a velocity larger than the velocity of sound in undisturbed water. Therefore, continuous expansion of the cavity leads to increasing density along the compressed water layer. This leads to the formation of the shock wave when the density of water behind the front of the disturbance is larger than the normal density. Because the expansion velocity of the cavity starts to decrease after the termination of the energy deposition into the wire, the generated shock detaches from the compressed layer. The latter results in the fast decrease in the shock velocity, because its divergence is accompanied by a corresponding decrease in the density behind the shock wave front. This phase continues till the shock velocity becomes equal to the velocity of sound in the compressed water layer between the shock front and the cavity. Indeed, the 1D HD simulations show that the shock velocity's fast

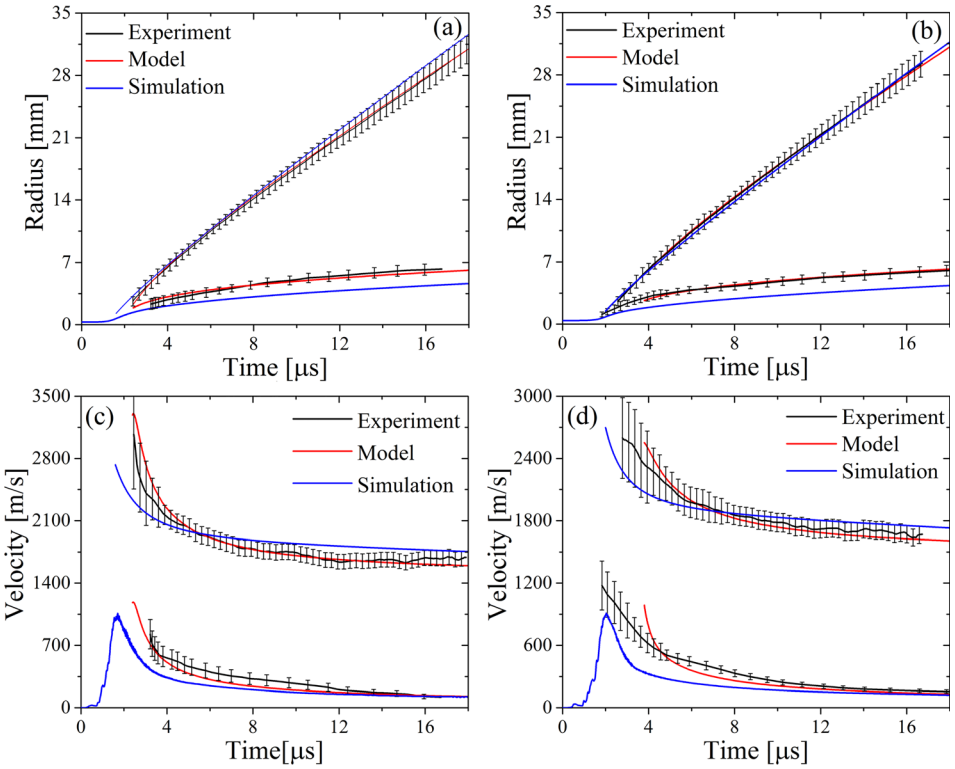

FIG. 5. Comparison of the experimental results (black solid), the simplified model (red solid), and 1D HD simulation (blue solid) for Cu 600 [(a) and (c)] and Al 800 [(b) and (d)] wire explosions.

decrease transforms into a gradual decrease when the velocity of sound in the compressed layer approaches the shock velocity.

One of the model's main assumptions is that the density of water inside the compressed layer at each instant of time is constant. However, the 1D HD simulations show a nonuniform radial distribution of the density behind the shock wave front at $t > 2\ \mu s$ (see Fig. 6). This apparent contradiction could be because, in the model, the shock wave velocity is determined by the density immediately behind shock front, calculated by the solution of the differential Eqs. (2), (4), and (6), coupled with the polytropic EOS for water using a 4th order Runge-Kutta algorithm. In the 1D HD simulations, the density behind the shock front is obtained as an averaged value for a given cell. Moreover, the shock wave front is smeared because of an artificial viscosity introduced for smoothing the shock. Here, let us note that the SESAME EOS has a relatively rough array of density values, which necessitate linear interpolation to find an appropriate value for the pressure. Thus, the comparative results of absolute density values from the 1D HD simulation and the simplified model should not be considered contradictory.

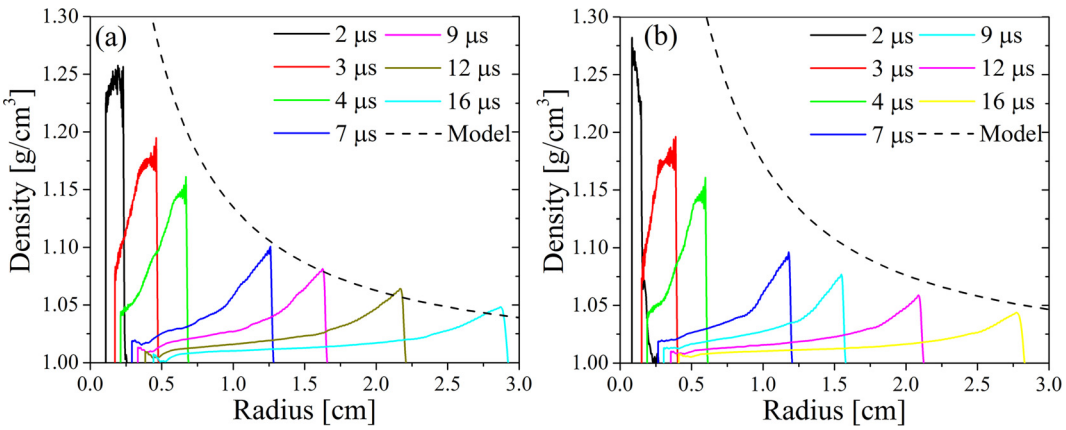

FIG. 6. Compressed layer's radial density distribution at different time steps for Cu 600 (a) and Al 800 (b) wire explosions calculated by 1D HD as compared with the model results for the density behind the shock wave front.

VI. SUMMARY

The results of the experimentally measured shock wave trajectories and the corresponding calculated velocities were compared with the results of the simplified model and verified by 1D HD simulations. It was shown that, despite the model's simplicity, which assumes uniform density inside the compressed water layer at each point in time, the experimental data agree with the model predictions when the velocity of the shock wave experiences a gradual decrease. The latter is explained by the continuous expansion of the plasma channel formed as a result of the wire explosion, which continuously supplies energy to the shock. It was also explained that the fast decrease in the shock velocity during the first few microseconds of its propagation is related to the subsonic dynamics of the exploded wire, which compresses the water layer at the wire's boundary.

ACKNOWLEDGMENTS

We thank Dr. J. Leopold for the critical reading of this manuscript and E. Flyat and S. Gleizer for generous technical assistance. This research was supported by the Center for Absorption in Science, Ministry of Immigrant Absorption, State of Israel and Israel Science Foundation, Grant No. 492/18.

REFERENCES

[1]V. E. Fortov and I. T. Iakubov, *The Physics of Non-Ideal Plasma* (World Scientific Publishing Co. Pte. Ltd., Singapore, 2000).
[2]B. A. Remington, R. P. Drake, and D. D. Ryutov, Rev. Mod. Phys. **78**, 755 (2006).
[3]G. Huser, M. Koening, A. Benuzzi-Mounaix, T. Vinci, B. Faral, M. Tomossini, B. Telaro, and D. Batani, Phys. Plasmas **12**, 060701 (2005).
[4]M. D. Knudson, D. L. Hanson, J. E. Bailey, C. A. Hall, J. R. Asay, and W. W. Anderson, Phys. Rev. Lett. **87**, 225501 (2001).
[5]Y. B. Zeldovich and Y. P. Raizer, *Physics of Shock Waves and High-Temperature Hydrodynamic Phenomena*, 2nd ed. (Academic Press, New York and London, 1966).
[6]G. B. Whitham, *Linear and Nonlinear Waves* (Wiley, New York, 1974).
[7]A. C. Mitchell and W. J. Nelilis, Rev. Sci. Instrum. **52**, 347 (1981).
[8]F. Amiranoff, R. Fedosejevs, R. F. Schmalz, R. Sigel, and Y.-l. Teng, Phys. Rev. A **32**, 3535 (1985).
[9]I. I. Komissarova, G. V. Ostrovskaya, V. N. Filippov, and E. N. Shedova, Zh. Tekh. Fiz. **67**, 138–140 (1997).
[10]V. A. Burtsev, N. V. Kalinin, and A. V. Luchinskii, *Electrical Explosion of Conductors and Its Applications* (Energoizdat, Moscow, 1990).
[11]G. I. Taylor, Proc. R. Soc. London, Ser. A **201**, 159 (1950).
[12]L. I. Sedov, Dokl. Akad. Nauk SSSR. **52**, 17–20 (1946).
[13]J. von Neumann, Ch. 2 Los Alamos Sci. Lab. Tech series, VII Pt. II (1947).
[14]G. Guderley, Luftfahrtforschung, Bd. **19**, S.302 (1942).
[15]L. D. Landau, J. Phys. Acad. Sci. USSR **9**, 496 (1945).
[16]K. P. Stanyukovich, *Unsteady Motion of Continuous Media* (Pergamon Press, Inc., New York, 1960).
[17]A. Sakurai, J. Phys. Soc. Jpn. **8**, 662 (1953).
[18]A. Sakurai, J. Phys. Soc. Jpn. **9**, 256 (1954).
[19]S. C. Lin, J. Appl. Phys. **25**, 54 (1954).
[20]F. D. Bennett, Phys. Fluids **1**, 347 (1958).
[21]D. L. Jones, G. G. Goyer, and M. N. Plooster, J. Geophys. Res. **73**, 3121, https://doi.org/10.1029/JB073i010p03121 (1968).
[22]G. C. Vlases and D. L. Jones, Phys. Fluids **9**, 478 (1966).
[23]Y. V. Skvortsov, V. S. Komelkov, and N. M. Kuznetsov, J. Tech. Phys. **30**(10), 1165–1177 (1960).
[24]E. V. Krivitskiy, V. K. Sholom, and V. P. Litvinenko, Elektron. Obrab. Mater. **4**, 38–42 (1975).
[25]E. V. Krivitskii, *Dinamika Elektrovzriva v Jidkosti* (Naukova Dumka, Kiev, 1986, in Russian).
[26]I. Z. Okun', J. Tech. Phys. **37**, 1729 (1967); I. Z. Okun', J. Tech. Phys. **39**, 837 (1969); **16**, 293 (1971); **41**, 303 (1971).
[27]E. V. Krivitskii and V. K. Sholom, Sov. Phys. - Tech. Phys. **19**, 798 (1974).
[28]A. W. DeSilva and J. D. Katsouros, Phys. Rev. E **57**, 5945 (1998).
[29]I. V. Lisitsyn, T. Muraki, and H. Akiyama, Jpn. J. Appl. Phys., Part 1 **36**, 1258 (1997).
[30]G. Rodriguez, J. P. Roberts, J. A. Echave, and A. J. Taylor, J. Appl. Phys. **93**, 1791 (2003).
[31]D. Yanuka, A. Rososhek, S. N. Bland, and Y. E. Krasik, Appl. Phys. Lett. **111**, 214103 (2017).
[32]O. Antonov, S. Efimov, D. Yanuka, M. Kozlov, V. T. Gurovich, and Y. E. Krasik, Appl. Phys. Lett. **102**, 124104 (2013).
[33]D. Yanuka, A. Rososhek, S. Efimov, M. Nitishinskiy, and Y. E. Krasik, Appl. Phys. Lett. **109**, 244101 (2016).
[34]E. M. Barkhudarov, M. O. Mdivnishvili, I. V. Sokolov, M. I. Taktakishvili, and V. E. Terekhin, J. Fluid Mech. **226**, 497–509 (1991).
[35]SESAME: *The Los Alamos National Laboratory Equation-of-State Database*, edited by S. P. Lyon and J. D. Johnson, Los Alamos National 347 Laboratory, Report No. LA-UR-92–3407, 1992.
[36]Y. E. Krasik, A. Grinenko, A. Sayapin, S. Efimov, A. Fedotov, V. T. Gurovich, and V. I. Oreshkin, IEEE Trans. Plasma Sci. **36**, C2 (2008).
[37]Y. E. Krasik, A. Fedotov, D. Sheftman, S. Efimov, A. Sayapin, V. T. Gurovich, D. Veksler, G. Bazalitski, S. Gleizer, A. Grinenko, and V. I. Oreshkin, Plasma Sources Sci. Technol. **19**, 034020 (2010).
[38]J. Lubbers and R. Graaff, Ultrasound Med. Biol. **24**(7), 1065–1068 (1998).
[39]A. Rososhek, S. Efimov, S. V. Tewari, D. Yanuka, K. Khishchenko, and Y. E. Krasik, Phys. Plasmas **25**, 062709 (2018).
[40]A. Rososhek, S. Efimov, S. V. Tewari, D. Yanuka, and Y. E. Krasik, Phys. Plasmas **25**, 102709 (2018).
[41]G. Bazalitski, V. T. Gurovich, A. Fedotov-Gefen, S. Efimov, and Y. E. Krasik, Int. J. Shock Waves, Detonations Explos. **21**, 321 (2011).
[42]L. Gilburd, S. Efimov, A. Fedotov Gefen, V. T. Gurovich, G. Bazalitski, O. Antonov, and Y. E. Krasik, Laser Part. Beams **30**, 215 (2012).
[43]S. Efimov, V. T. Gurovich, G. Bazalitski, A. Fedotov, and Y. E. Krasik, J. Appl. Phys. **106**, 073308 (2009).